Progress In Electromagnetics Research C, Vol. 136, 245–259, 2023

Study on Sensorless Control of Six Phase Fault-Tolerant Permanent Magnet Rim Driven Motor with Improved Second-Order SOGI HF Voltage Injection

Yonghan Liu, Jingwei Zhu*, Ping Ren, Jiang Wu, and Si Chen

Abstract—From the perspective of motor control and manufacturing process, the application of fault-tolerant permanent magnet rim driven motor (FTPM-RDM) in shaftless rim driven thruster (RDT) can avoid complicated shafting structure in traditional propulsion system effectively and realize sensorless control while reducing volume. Referring to fault-tolerant structure features, this paper introduces an improved sensorless control algorithm based on two-stage second-order generalized integral (SOGI) pulsating high-frequency (HF) voltage injection which is applied to the FTPM-RDM in zero and low speed. This algorithm can realize the rotor position estimation under fault and healthy condition. Based on pulsating HF injection method, HF square-wave voltages are injected in the virtual dq axis, and the initial rotor position can be extracted from the response currents of stationary reference frame (SRF). The sinusoidal voltage is injected into the virtual dq axis, and use two-stage SOGI instead of the traditional filter is used to realize the current modulation without delay in low speed rotor position estimation. Combining the simulation and experiments, the proposed sensorless control strategy can estimate the rotor position accurately whether in failure or not and has good dynamic and static performance.

1. INTRODUCTION

With the rapid development of ship technology, the performance of marine power plant is becoming more and more important as the primary sector of the ship. As a new type of marine propeller, shaftless RDT eliminates the requirement of torque transmission using traditional shaft. It increases the propulsion efficiency effectively by integrating the motor with the propeller [1–3]. Currently both of the permanent magnet synchronous motors (PMSMs) and switched reluctance motors (SRMs) can be applied to RDM [4, 5]. However, the traditional PMSM has limited fault tolerance, which may make the motor unable to function properly when the inverter fails [6]. Therefore, different forms of multiphase PMSM drives are widely used for its high efficiency, small size and low torque ripple. FTPM-RDM is a new type of dual three-phase (DTP) PMSM which is symmetrically displaced by 60 degrees electrically. It is settled upon isolated phase winding design, and each phase is driven by an independent H-bridge inverter circuit, which is still able to work in the event of one or more phases open circuit [7–9]. Therefore, RDT can improve the reliability and safety by adopting FTPM-RDM in RDT system. The position sensor cannot be installed due to the shaftless structure of FTPM-RDM. Sensorless control technology of DTP PMSM has been widely concerned and applied [9–12]. It is divided into two categories according to its appropriate conditions: control strategies for medium-high speed operation and for zero-low speed operation [13]. The rotor position in medium-high speed is extracted mainly by Back-EMF while the signal to noise ratio (SNR) which is used to extract voltage is small in

Received 17 July 2023, Accepted 10 August 2023, Scheduled 23 August 2023
* Corresponding author: Jingwei Zhu (zjwdl@dlmu.edu.cn).
The authors are with the College of Marine Electrical Engineering, Dalian Maritime University, Dalian 116026, China.

zero-low speed, and it is difficult to obtain position information [14]. The control strategy for zero-low speed mainly utilizes the salient structure, and it is easy to estimate the rotor position by means of salient information and signal separation [15].

Open loop start method and high frequency (HF) injection method are widely used in position sensorless control under zero-low speed condition. In open loop start method, the deviation between estimated position and actual position in practical application is small. But what position the rotor is pulled to when the position is predetermined and time of the movement also need to be considered. In addition, the reversal phenomenon which is easy to occur in the process will affect the control accuracy [16]. The HF injection method is mainly classified as HF rotating voltage signal injection, HF square-wave voltage injection, and HF pulse signal injection according to the input waveform. The HF sine wave voltage signal injection is divided into rotating HF voltage signal injection and fluctuating HF voltage injection [17]. [18] injects the rotating HF voltage into a two-phase stationary coordinate system (SCS) and obtains the rotor position information from the phase hidden in the response current. The system has high stability due to the sine wave voltage injected which can also brings torque ripple and current fluctuation inevitably. In traditional fluctuating HF voltage injection method, lowpass filter (LPF) is used to extract the response current signal. Although the HF signal can be basically filtered out when the order of the filter is set high enough, it will cause the current signal phase delay [19]. In [20], a second-order generalized integrator is used instead of a bandpass filter to extract HF voltage signals, and a specific frequency harmonic cancellation unit replaces the LPF to obtain rotor position error signals, which improves the dynamic performance of the motor drive system. In [21], an HF square wave voltage injection method based on phase locked loop (PLL) is used to eliminate the LPF remodulation process to obtain the rotor position information. The proposed method eliminates the complicated dq coordinate transformation. It can also independently control two motors with no additional external circuit.

The fault-tolerant control technology of FTPM-RDM is one of the important research directions of drive system. At present, single-phase failure is the most common fault type. The current fault-tolerant strategy of FTPMM base on vector space decomposition (VSD) is proposed in [22]. The fault-tolerant capability of FTPMM is improved by introducing fault compensation control strategy and considering the change of equivalent harmonic inductance. The fault-tolerant strategy of five-phase FTPMM is proposed in [23], and the optimal fault-tolerant current of FTPM-RDM based on the fundamental wave reduced order matrix is constructed to ensure the magnetomotive force conservation in the fault state and output stable torque.

Based on the fault-tolerant structure of FTPM-RDM, an improved zero-low speed sensorless control strategy is proposed in this paper. First, with injecting HF square wave voltage into the virtual dq axis, the initial rotor position is obtained by detecting the $\alpha\beta$ axis response current and judging whether the quadrant where the rotor position is located needs compensation according to its sign (positive and negative). Second, the rotor position is obtained based on two-stage SOGI method during low speed. The front stage SOGI replaces BPF to reduce current distortion and extract HF response current. The post stage SOGI replaces LPF to solve current phase delay and obtain estimated rotor position information. Finally, combined with the current fault tolerant control strategy, an experimental platform is built to verify the correctness and effectiveness of the proposed algorithm.

2. THE STRUCTURE AND MATHEMATICAL MODEL OF FTPM-RDM

The six-phase FTPM-RDM adopts the integrated structure of motor and propeller. In order to improve the propulsion efficiency and increase the propeller diameter as much as possible, a surface-mounted permanent magnet rotor is selected as the driving structure. Figure 1 shows the topological structure of FTPM-RDM.

The stator of the motor uses single-layer concentrated winding and the isolation teeth between phases which can effectively avoid the effect of electrical coupling on other phases under failure conditions. The six-phase FTPM-RDM is driven by six independent H-bridge inverter circuit to improve the fault-tolerant performance, and there is no neutral link in the circuit. The structure of the circuit is shown in Figure 2. This structure can inhibit the short circuit current generated by the short circuit fault. Therefore, the internal and external design of the motor can not only achieve physical isolation and thermal isolation, but also achieve magnetic isolation and electrical isolation.

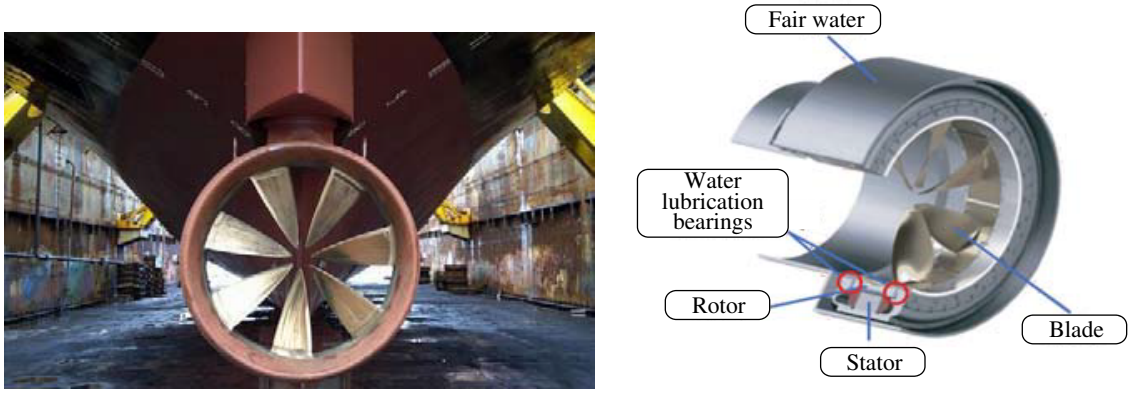

Figure 1. The physical map and structural diagram of FTPM-RDM.

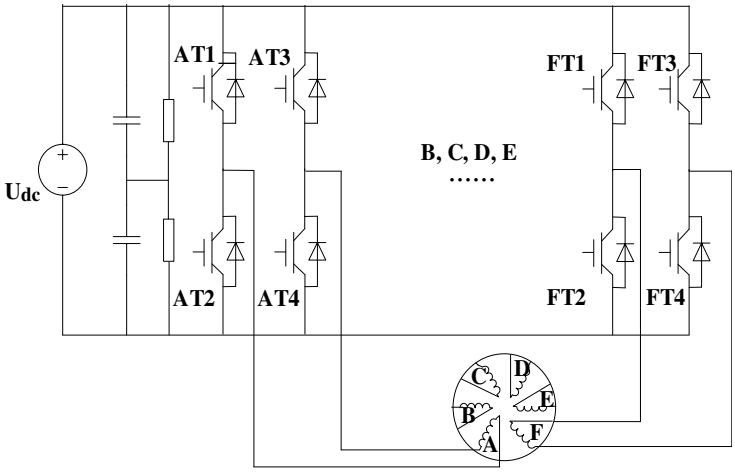

Figure 2. The diagram of H-bridge inverter circuit for six-phase FTPM-RDM.

The voltage equation of FTPMV-RDM in six-phase stationary reference frame (SRF) can be expressed as:

$$u_s = R_s i_s + \frac{\mathrm{d}}{\mathrm{d}t}\left[L_s i_s + \psi_s \cos\left(\theta + \sigma_s\right)\right] \tag{1}$$

where u_s, R_s, i_s, ψ_s, L_s, σ_s are the voltage, resistance, current, flux linkage, inductance, and angle relative to phase A of each phase stator winding. "s" is represented by "A, B, C, D, E, F". By transforming it into the $\alpha\beta$ SRF, the voltage equation of FTPM-RDM can be obtained as follows:

$$u_{\alpha\beta} = R_s i_{\alpha\beta} + \frac{\mathrm{d}\psi_{\alpha\beta}}{\mathrm{d}t} \tag{2}$$

where $u_{\alpha\beta}$, $i_{\alpha\beta}$, and $\psi_{\alpha\beta}$ represent the voltages, currents and flux linkages of α axis and β axis in the $\alpha\beta$ SRF. The flux linkage equation of FTPM-RDM in $\alpha\beta$ SRF can be expressed as:

$$\psi_{\alpha\beta} = L_s i_{\alpha\beta} + \sqrt{\frac{3}{2}}\,\psi_f \frac{\mathrm{d}}{\mathrm{d}t}\begin{bmatrix}\cos\theta \\ \sin\theta\end{bmatrix} \tag{3}$$

where ψ_f is the permanent flux. In order to make the control convenient and simple, the equation is transformed from the $\alpha\beta$ SRF to dq rotating reference frame (RRF). The voltage equation is:

$$u_{dq} = R_s i_{dq} + \frac{\mathrm{d}\psi_{dq}}{\mathrm{d}t} + \omega\psi_{dq} \tag{4}$$

where u_{dq}, i_{dq}, ψ_{qd}, ω represent the voltages, currents, flux linkages, and electrical angle of d axis and q axis in the RRF. The flux linkage equation is:

$$\begin{aligned} \psi_d &= L_d i_d + \sqrt{\frac{3}{2}}\psi_f \\ \psi_q &= L_q i_q \end{aligned} \tag{5}$$

where L_d, L_q are the inductances of dq axis. The electromagnetic torque can be expressed as:

$$T_e = n_p\left(\psi_d i_q - \psi_q i_d\right) \tag{6}$$

3. ROTOR POSITION ESTIMATION

3.1. Improved Initial Position Estimation Method

The initial position calculation of FTPM-RDM based on pulsating HF voltage signal injection is proposed to avoid the impact of multiple filters which is used in the rotary signal injection method on inaccurate detection.

The inductance of the motor increases with the injection of HF voltage, and the stator resistance of the motor can be ignored compared with the motor impedance, that is $R_s \ll Z$. The simplified voltage equation can be expressed as:

$$u_{dq} = L_{dq}\frac{\mathrm{d}i_{dq}}{\mathrm{d}t} \tag{7}$$

The principle of HF voltage injection is to inject HF voltage into the d-axis to produce changes in d-axis inductance, then extract the rotor position information by saturation saliency effect. According to the relationship between real and estimated rotor positions in RRF, as shown in Figure 3. θ is the real rotor position. $\hat{\theta}$ is the estimated rotor position. $\Delta\theta = \theta - \hat{\theta}$ is the rotor position error.

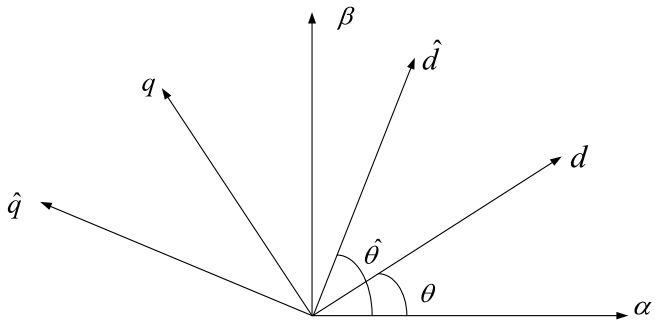

Figure 3. Real and estimated rotor synchronous RRF relationship diagram.

The HF voltage signal injected in $\hat{d}$-axis is:

$$\begin{bmatrix} u_{\hat{d}h} \\ u_{\hat{q}h} \end{bmatrix} = \begin{bmatrix} u \\ 0 \end{bmatrix} \tag{8}$$

In Equation (8):

$$u = \begin{cases} U, t \in \left[nT, \left(n+\dfrac{1}{2}\right)T\right] \\ -U, t \in \left[\left(n+\dfrac{1}{2}\right)T, (n+1)T\right] \end{cases} \tag{9}$$

where $u_{\hat{d}h}$ and $u_{\hat{q}h}$ are the voltages injected in $\hat{d}$ axis and $\hat{q}$ axis of the estimated RRF. U and T are the amplitude and period of the injected voltage. Transform Equation (8) into dq axis, and the voltage

equation of the real dq axis can be obtained as follows:

$$\begin{bmatrix} u_{dh} \\ u_{qh} \end{bmatrix} = \begin{bmatrix} \cos\Delta\theta & \sin\Delta\theta \\ -\sin\Delta\theta & \cos\Delta\theta \end{bmatrix} \begin{bmatrix} u_{\hat{d}h} \\ u_{\hat{q}h} \end{bmatrix} \tag{10}$$

where u_{dh} and u_{qh} are the voltages injected in d axis and q axis of the real RRF.

The current equation in real dq axis can be expressed as:

$$\begin{bmatrix} i_{dh} \\ i_{qh} \end{bmatrix} = \begin{bmatrix} \cos\theta & \sin\theta \\ -\sin\theta & \cos\theta \end{bmatrix} \begin{bmatrix} i_{\alpha h} \\ i_{\beta h} \end{bmatrix} \tag{11}$$

where i_{dh}, i_{qh} are the real dq axis currents. $i_{\alpha h}$, $i_{\beta h}$ are the currents in $\alpha\beta$ SRF. Plug (8)$\sim$(11) into (7):

$$\begin{bmatrix} \dfrac{di_{\alpha h}}{dt} \\ \dfrac{di_{\beta h}}{dt} \end{bmatrix} = u \begin{bmatrix} \dfrac{\cos\theta\cos\Delta\theta}{L_d} + \dfrac{\sin\theta\sin\Delta\theta}{L_q} \\ \dfrac{\sin\theta\cos\Delta\theta}{L_d} + \dfrac{\cos\theta\sin\Delta\theta}{L_q} \end{bmatrix} \tag{12}$$

From Equation (12), the rotor position can be obtained from the differential currents in $\alpha\beta$ SRF. In surface mounted FTPM-RDM, $L_d = L_q = L$, then Equation (12) can be simplified as:

$$\begin{bmatrix} \dfrac{di_{\alpha h}}{dt} \\ \dfrac{di_{\beta h}}{dt} \end{bmatrix} = \frac{u}{L} \begin{bmatrix} \cos\theta \\ \sin\theta \end{bmatrix} \tag{13}$$

Define new variables $\dot{i}_{\alpha h}$, $\dot{i}_{\beta h}$ to calculate the rotor position. Equation (13) can be rewritten as:

$$\begin{bmatrix} \dot{i}_{\alpha h} \\ \dot{i}_{\beta h} \end{bmatrix} = \begin{bmatrix} \cos\theta \\ \sin\theta \end{bmatrix} \tag{14}$$

The position error ξ can be calculated by the trigonometric function:

$$\xi = \dot{i}_{\alpha h}\sin\hat{\theta} - \dot{i}_{\beta h}\cos\hat{\theta} = \sin\Delta\theta \tag{15}$$

When ξ is extremely small, $\sin\Delta\theta \approx \Delta\theta$, then the rotor position error can be simplified as:

$$\xi \approx \Delta\theta \tag{16}$$

The PI position tracker is used to adjust the current error ξ. The estimated rotor position will coincide with the actual value by adjusting the value of ξ to zero, and the initial angle of the estimated rotor position can be obtained. However, the signs of $\cos\theta$ and $\sin\theta$ in $\alpha\beta$ axis are different in the four-quadrant which may cause heavy error in initial position detection. Therefore, a novel method of position compensation based on the sign of $\cos\theta$, $\sin\theta$ is proposed:

1) $i_{\alpha h} > 0, i_{\beta h} > 0$, the rotor position is in the first quadrant, $\theta = \theta'$.
2) $i_{\alpha h} < 0$, the rotor position is in the second or third quadrant, $\theta = \theta' + \pi$.
3) $i_{\beta h} < 0$, $i_{\alpha h} > 0$, the rotor position is in the forth quadrant, $\theta = \theta' + 2\pi$.

where θ is the compensated rotor position. θ' is the uncompensated rotor position.

3.2. Improved Low Speed Position Estimation Method

From Figure 3, when HF voltage signal is injected into the RRF of FTPM-RDM, the voltage model can be expressed as (10), and the current model can be expressed as follows:

$$\begin{bmatrix} i_{dh} \\ i_{qh} \end{bmatrix} = \begin{bmatrix} \cos\Delta\theta & \sin\Delta\theta \\ -\sin\Delta\theta & \cos\Delta\theta \end{bmatrix} \begin{bmatrix} i_{\hat{d}h} \\ i_{\hat{q}h} \end{bmatrix} \tag{17}$$

where $i_{\hat{d}h}$, $i_{\hat{q}h}$ are the response currents in $\hat{d}\hat{q}$ RRF. From Equations (7), (10), and (17), the relation between voltage and current in $\hat{d}\hat{q}$ axis is represented as shown below.

$$\begin{bmatrix} u_{\hat{d}h} \\ u_{\hat{q}h} \end{bmatrix} = \begin{bmatrix} L_1 + L_2\cos 2\Delta\theta & L_2\sin 2\Delta\theta \\ L_2\sin 2\Delta\theta & L_1 - L_2\cos 2\Delta\theta \end{bmatrix} \begin{bmatrix} \dfrac{di_{\hat{d}h}}{dt} \\ \dfrac{di_{\hat{q}h}}{dt} \end{bmatrix} \tag{18}$$

where $L_1 = (L_d + L_q)/2$ is the average inductance; $L_1 = (L_d - L_q)/2$ is the difference inductance. Equation (18) is the HF voltage signal which is injected into the estimated RRF.

$$\begin{bmatrix} u_{\hat{d}h} \\ u_{\hat{q}h} \end{bmatrix} = \begin{bmatrix} U_h\cos\omega_h t \\ 0 \end{bmatrix} \tag{19}$$

where U_h is the amplitude of the injected voltage, and ω_h is the frequency of the injected voltage. Combining Equations (18) and (19), the response currents of the estimated RRF can be calculated and expressed as follows:

$$\begin{bmatrix} i_{\hat{d}h} \\ i_{\hat{q}h} \end{bmatrix} = \frac{U_h\sin\omega_h t}{\omega_h(L_1^2 - L_2^2)} \begin{bmatrix} L_1 - L_2\cos 2\Delta\theta \\ -L_2\sin 2\Delta\theta \end{bmatrix} \tag{20}$$

Equation (20) has the error information of rotor position. Therefore, the estimated rotor position can be obtained through the position extraction step. Figure 4 shows the rotor position information extraction process.

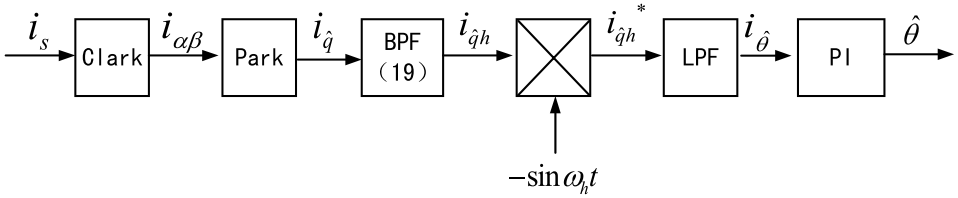

Figure 4. Rotor position extraction structure based on traditional LPF.

From Figure 4, the modulated current $i_{\hat{q}h}^*$ can be obtained by multiplying the response currents by $-\sin\omega_h t$. $i_{\hat{q}h}^*$ is represented as:

$$i_{\hat{q}h}^* = i_{\hat{q}h}(-\sin\omega_h t) = \frac{U_h L_2}{\omega_h(L_1^2 - L_2^2)}\sin 2\Delta\theta(\sin\omega_h t)^2 = \frac{U_h L_2}{\omega_h(L_1^2 - L_2^2)}\sin 2\Delta\theta\left(\frac{1}{2} - \frac{1}{2}\cos 2\omega_h t\right) \tag{21}$$

In traditional rotor position extraction algorithm, the HF component of Equation (21) can be eliminated by LPF. Therefore, the expression of the low frequency current component $i_{\hat{\theta}}$, including the rotor position error information after filtering, is as follows:

$$\begin{aligned} i_{\hat{\theta}} &= \mathrm{LPF}(i_{\hat{q}h}^*) = \frac{U_h L_2}{\omega_h(L_1^2 - L_2^2)}\sin 2\Delta\theta * \mathrm{LPF}\left(\frac{1}{2} - \frac{1}{2}\cos 2\omega_h t\right) \\ &= \frac{U_h L_2}{2\omega_h(L_1^2 - L_2^2)}\sin 2\Delta\theta \approx \frac{U_h L_2}{\omega_h(L_1^2 - L_2^2)}\Delta\theta \end{aligned} \tag{22}$$

Finally, the real estimated rotor position can be obtained by PI regulator or other techniques.

Using LPF to extract rotor position can filter out HF fluctuations, but there will be a delay which can cause large error in rotor position compared with the original signal. In order to solve the problem of current distortion caused by BPF and signal delay caused by LPF, a band-pass filter based on second-order generalized integral (SOGI) is proposed in this paper. Its structure is shown in Figure 5, and the transfer function can be expressed as follows:

$$\mathrm{SOGI}(s) = \frac{i_{\hat{q}h}}{k_1\tilde{i}_{\hat{q}}}(s) = \frac{\omega_h s}{s^2 + \omega_h^2} i_{\hat{q}h} \tag{23}$$

$$\frac{i_{\hat{q}h}}{i_{\hat{q}}} = \frac{k_1\omega_h s}{s^2 + k_1\omega_h s + \omega_h^2} \tag{24}$$

$$\tilde{i}_{\hat{q}} = i_{\hat{q}h} - i_{\hat{q}} \tag{25}$$

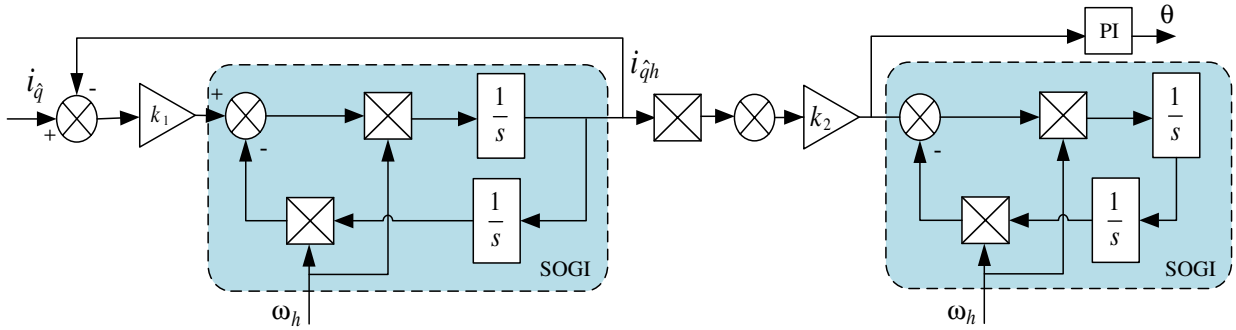

Figure 5. Basic structure of SOGI.

According to Figure 5, a two-stage SOGI is used to extract rotor position information in this paper. One is to replace BPF to extract HF component of $\hat{q}$-axis current, and the other is to replace LPF to extract the DC component of $i^*_{\hat{q}h}$ which contains the position information. The new modulated response current can be expressed as:

$$\begin{aligned} i^*_{\hat{q}h} &= i_{\hat{q}h}(-\sin\omega_h t) = \frac{U_h \sin\omega_h t(-L_2 \sin 2\Delta\theta)}{\omega_h(L_1^2 - L_2^2)} * (-\sin\omega_h t) \\ &= \frac{U_h L_2}{2\omega_h(L_1^2 - L_2^2)} \sin 2\Delta\theta - \frac{U_h L_2}{2\omega_h(L_1^2 - L_2^2)} \cos 2\omega_h t \end{aligned} \tag{26}$$

The signal $i_{\hat{\theta}}$ which contains rotor position error information can be extracted by the second SOGI. The expression of the new signal $i_{\hat{\theta}}$ is as follows:

$$i_{\hat{\theta}} = \text{SOGI}(i^*_{\hat{q}h}) = \frac{U_h L_2}{2\omega_h(L_1^2 - L_2^2)} \sin 2\Delta\theta \tag{27}$$

where k_1 and k_2 are the filter gains. The rotor position can be estimated by using the PI regulator after obtaining $i_{\hat{\theta}}$.

The current vector faut-tolerant (CVFT) compensation method used in [24] is selected as the fault-tolerant strategy use in this paper. Figure 6 is a detailed control block diagram of FTPM-RDM system based on improved HF injection method. In this control strategy, the FTPM-RDM that adopts the fault-tolerant method described above can still estimate the rotor position on the condition of one phase open circuit.

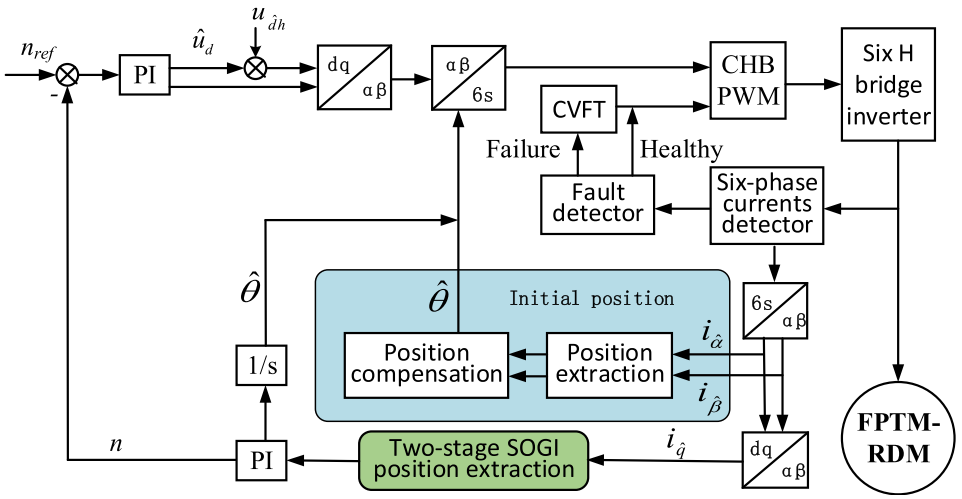

Figure 6. Sensorless control system of FTPM-RDM based on HF injection method.

4. SIMULATION VERIFICATION

Establishing a simulink model in use of Matlab/Simulink to verify the feasibility of the proposed algorithm. The parameters of the six-phase FTPM-RDM in the simulation are shown in Table 1. The sampling frequency of the simulation model is set as 10 kHz to make sure that the simulation effect satisfies the request of actual application.

Table 1. FTPM-RDM simulation experiment parameters.

Parameters	value
Stator resistance R, (Ω)	1.2
Number of pole-pairs np	15
Winding inductance L, (mH)	27.42
Rated torque T, ($N \cdot$ m)	23.87
Rated power P, (kW)	1.5
Rated speed N, (r/min)	600
Rotational inertia J, (kg $\cdot$ m^2)	0.05

4.1. Zero Speed Simulation

In order to verify the position compensation effect at zero speed, the initial rotor position is set to 2 rad, located in the second quadrant. The voltage amplitude of the HF square wave injected in $\hat{d}$-axis is 2 V, and its frequency is 1 kHz. The estimated rotor position and actual position before and after compensation are shown in Figure 7. The estimated rotor position in this quadrant should compensate π according to the algorithm above. Figure 7 verifies the effectiveness of compensation method. The estimated position is basically consistent with the real position after compensation. The magnified portion of a section in Fig. 7 showing the maximum error is only 1.7°.

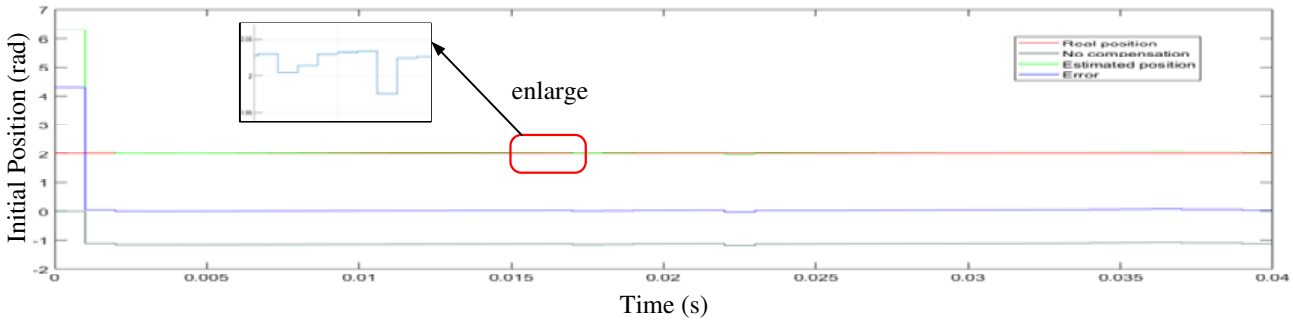

Figure 7. Comparison between the actual rotor position and estimated rotor position in 2 rad.

4.2. Low Speed Simulation

The voltage amplitude of the HF sine wave injected in RRF is 20 V, and its frequency is 1 kHz. The simulation is divided into two parts, healthy and no fault condition, specifically as follows.

4.2.1. Simulation Results under Healthy Condition

Figure 8 shows the estimated position diagram of the HF injection based on SOGI compared with the actual position. The FTPM-RDM operates stably at 50 r/min in unloading condition. The error

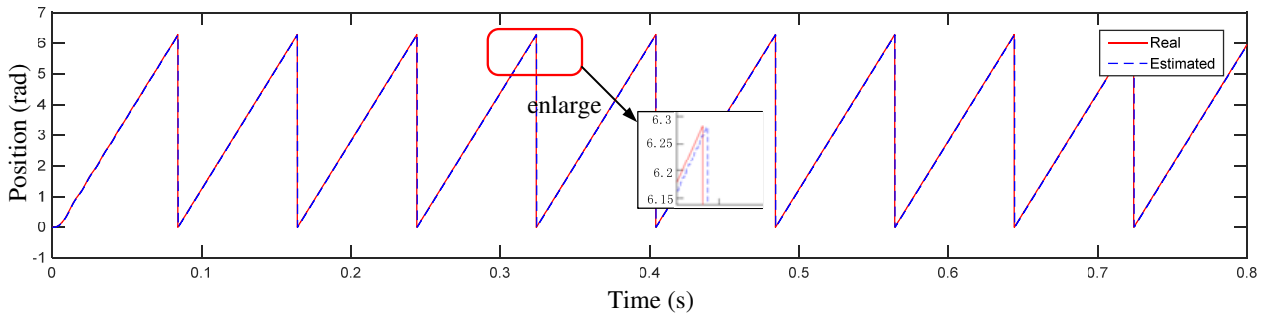

Figure 8. Simulation results of FTPM-RDM speed at 50 r/min.

between the two position is within 0.05 rad. The result shows that the method has a good static performance.

Figure 9 shows the dynamic characteristic of the FTPM-RDM running at zero-load condition using HF voltage injection method. The motor starts in the condition of 20 r/min with abrupt change of 40 r/min at 0.5 s. It can be seen from the results that when the speed changes, the method of estimating rotor position based on SOGI HF voltage injection can estimate rotor position effectively. Its average rotor position estimation error is about 2°, which is smaller than the average estimation error 8° based on LPF before improvement.

4.2.2. Simulation Results under One-phase Open Circuit Condition

Figure 10 shows the estimated rotor position by using modified position estimation method under one-phase open circuit condition. For simulating the FTPM-RDM under fault condition we have two methods, namely VSD and CVFT, and CVFT is used in this paper. The given speed of the motor is 50 r/min, and it works under 10 Nm load. An open circuit fault occurs in phase A, and the fault tolerant control strategy is added at 0.6 s. The actual and estimated rotor positions and the error between the two positions are shown in Figs. 10(a) and (b), respectively. The rotor position estimation based on SOGI HF injection method can track the actual rotor position well under malfunction in the image. The rotor position error is stabilized at 6° after failure. This method has good fault tolerance and dynamic performance.

5. EXPERIMENT VERIFICATION

In this paper, the validity of the proposed control strategy is verified by the six-phase FTPM-RDM vector control system hardware experiment platform as shown in Figure 11. This platform mainly includes six-phase FTPM-RDM, motor controller, hardware circuit, and upper computer. Fast control prototype rapid control prototyping (RCP) is selected as the core controller of motor control. The motor parameters used in the experiment are the same as thsoe used in MATLAB. The hardware sampling frequency is 10 kHz. The amplitude of the injection voltage is 20 V, and its frequency is 1 kHz.

The experiment of rotor position estimation is specifically set to the steady state operation and the step-speed dynamic operation. Furthermore, an open circuit fault of phase A is simulated during the dynamic operation, and the change of the estimated rotor position error is observed by adding fault tolerant strategy.

5.1. Analysis of Steady-State Operation Experiment Result

Figure 12 and Figure 13 show the speed and rotor position result of improved estimation algorithm based on SOGI HF injection. The motor operates at stable speeds of 50 r/min with 10 Nm load under fault-free condition. The estimated position can track the actual position stably. And the error between them is within 0.003°. The result suggests that this method can be applied to the stable operation of FTPM-RDM at low speed.

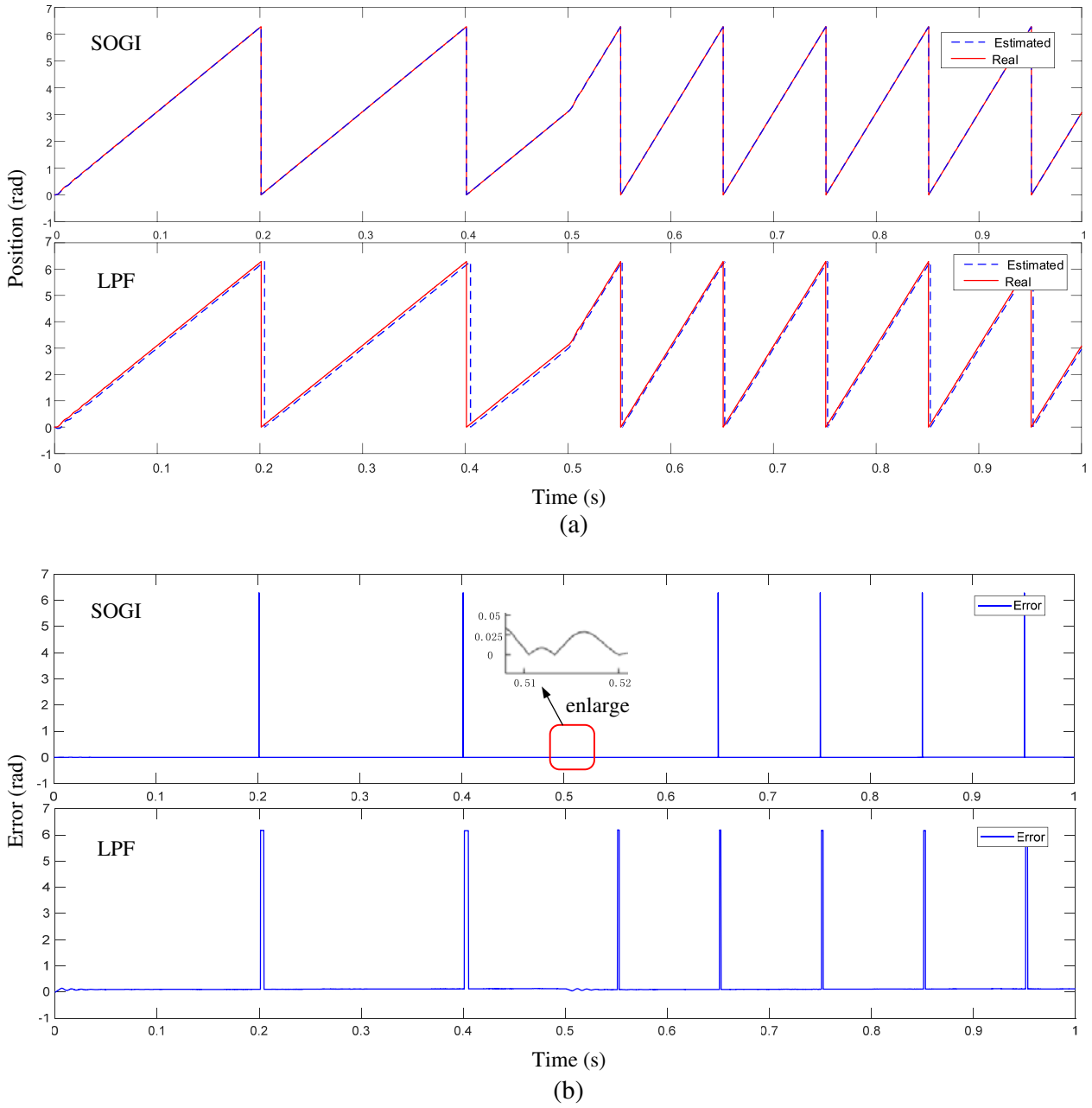

Figure 9. Comparison results of rotor position by two HF injection methods in FTPM-RDM. (a) The estimated rotor position and the actual position. (b) The error of estimated rotor position.

5.2. Analysis of Dynamic Operation Experiment Result

5.2.1. Experiment Results under Healthy Condition

The experiments using SOGI HF injection method under healthy condition are carried out. Figure 14 shows the dynamic characteristic of the FTPM-RDM using HF injection method. The motor starts at 40 r/min with abrupt change of 60 r/min at some point. It can be seen from the results that when the speed changes, the method of estimating rotor position based on SOGI HF injection can estimate rotor position accurately. Its average speed estimation error is within 1 r/min, and rotor position estimation error is about 2°. The improved estimated rotor position error is larger but within the allowable range as the speed changes instantaneously. The estimated rotor position can track the speed changes

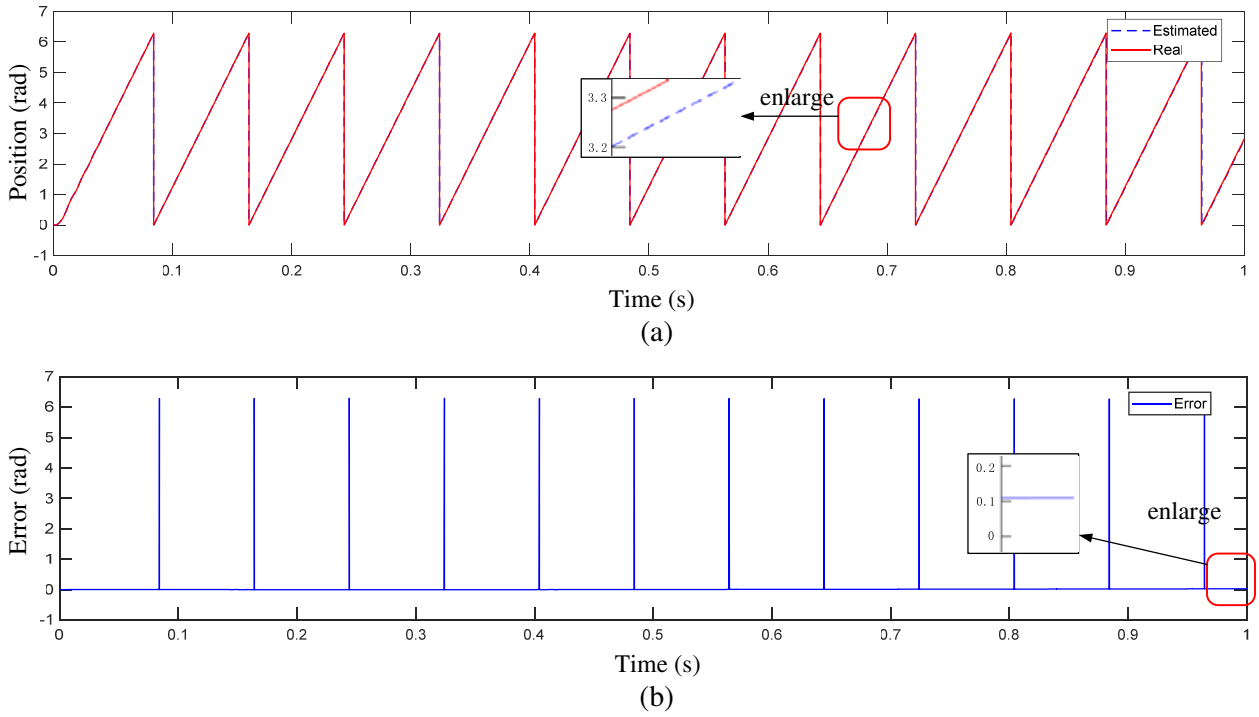

Figure 10. Rotor position simulation based on SOGI HF injection method in the condition of phase A open circuit. (a) The estimated rotor position and the actual position. (b) The error of estimated rotor position.

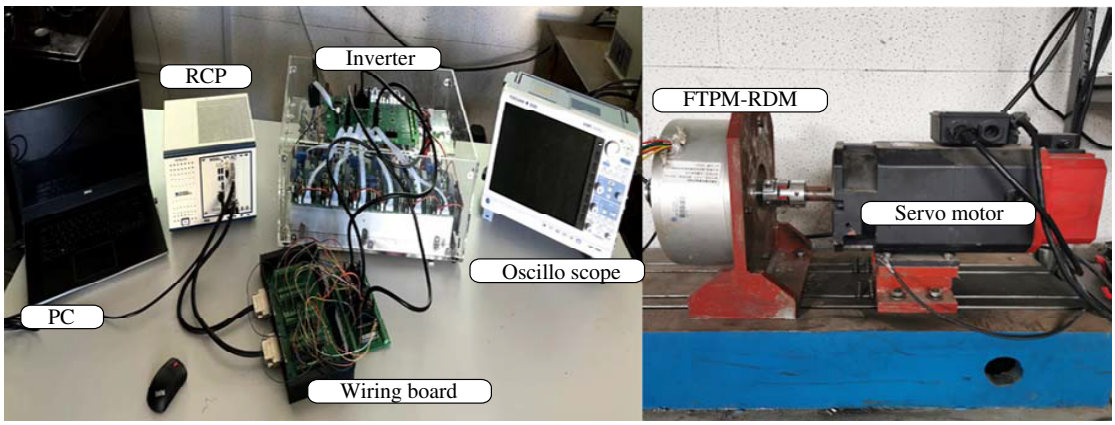

Figure 11. FTPM-RDM hardware experimental platform.

quickly and reposition the rotor position within 0.1 s without misalignment, proving its good response characteristic.

5.2.2. Experiment Results under One-Phase Open Circuit Condition

The FTPM-RDM runs at a constant speed of 40 r/min with 10 Nm in use of SOGI HF injection method. Phase A winding will open at some point. The changes of the actual position, estimated position, and position error are shown in Figure 15. As shown in the figure, the estimated position error is around 10° after phase A open circuit. Although the error is large, the motor can still run stably, which indicates

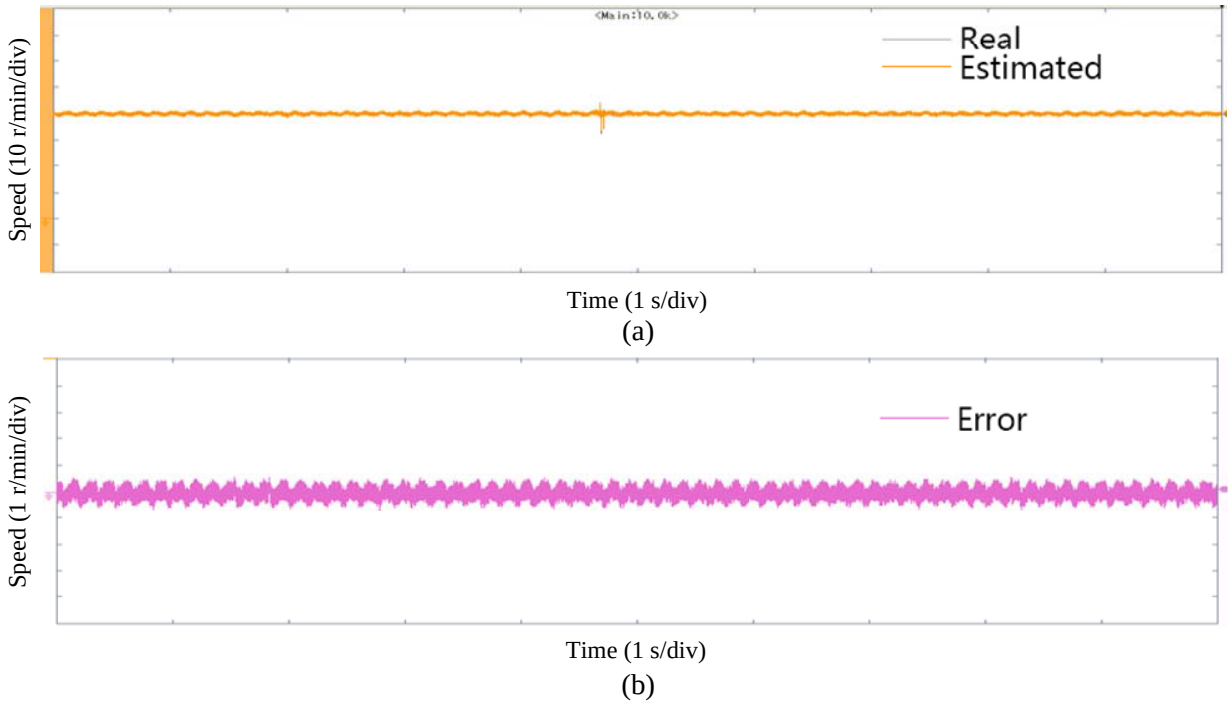

Figure 12. Experimental verification results of FTPM-RDM speed at 50 r/min. (a) The estimated speed and the actual speed. (b) The error of estimated speed.

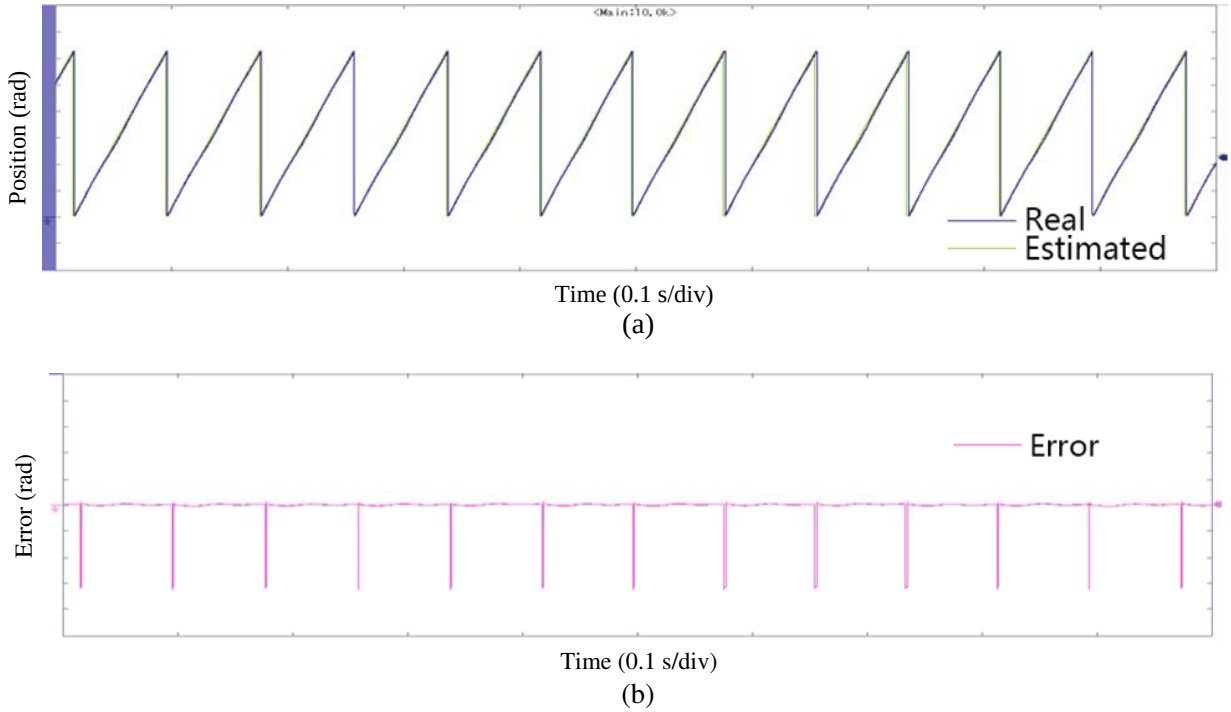

Figure 13. Experimental verification results of FTPM-RDM rotor position at 50 r/min. (a) The estimated rotor position and the actual position. (b) The error of estimated rotor position.

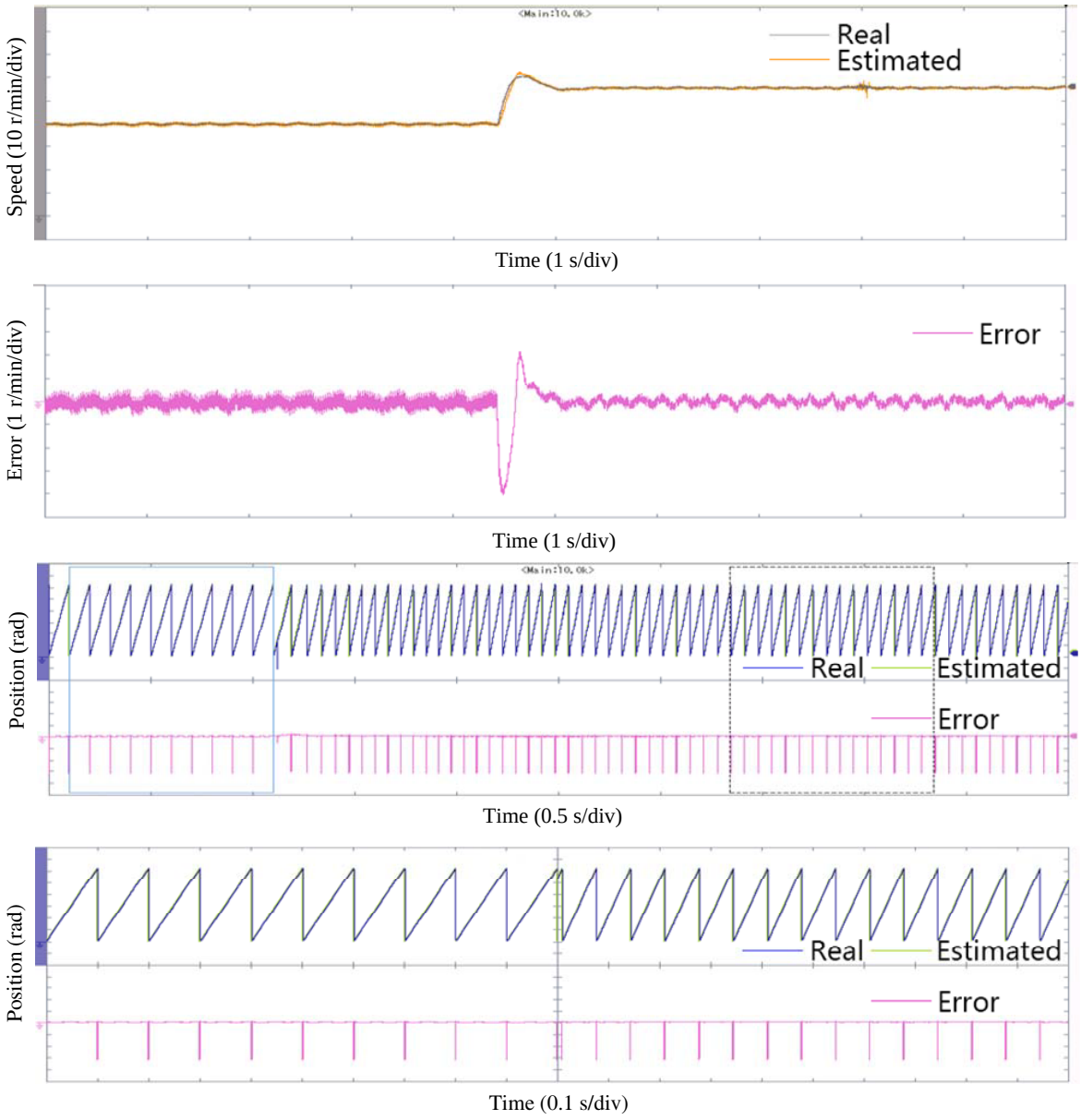

Figure 14. The step-speed experiment results of rotor position estimation by SOGI HF method.

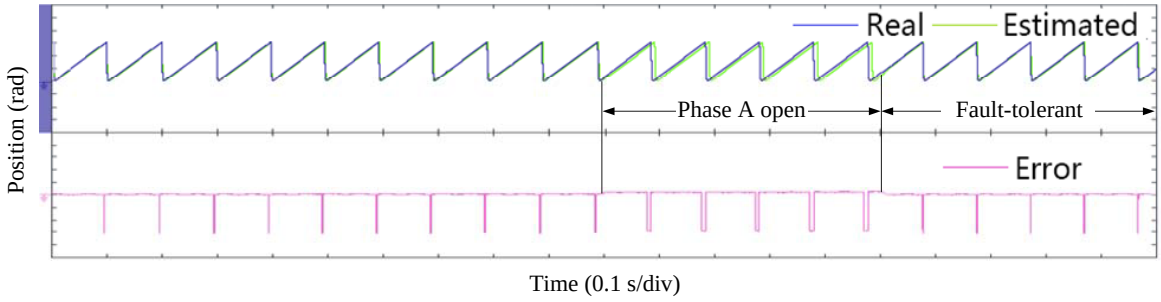

Figure 15. The rotor position estimation algorithm based on fault-tolerant control strategy is verified by experiments.

that the method is suitable for the fault condition of one phase open circuit. The motor can return to steady running condition quickly when adding fault tolerant control strategy, and the rotor position error is about 2°. This experiment result shows that the method combining SOGI HF injection and fault tolerant strategy can achieve accurate and fast rotor position estimation under fault condition.

6. CONCLUSION

In this paper, an improved sensorless control algorithm based on two-stage SOGI pulsating HF voltage injection which is applied to the FTPM-RDM in zero and low speed realizes the rotor position estimation under fault and healthy condition introduced. This method not only achieves accurate estimation of rotor position at zero speed, with the maximum error 1.7° but also realizes the current modulation without delay in low speed rotor position estimation. Combining the simulation and experiments, the proposed sensorless control strategy can estimate the rotor position accurately whether in failure or not and has good dynamic and static performance. This method has great significance for further research on FTPM-RDM sensorless control technology.

ACKNOWLEDGMENT

This work was supported in part by the National Natural Science Foundation of China under Grant 51777024, in part by the Stability Support Project of the Laboratory of Science and Technology on Integrated Logistics Support, National University of Defense Technology under Grant WDZC20235250309.

REFERENCES

1. Yang, Z., X. Yan, and W. Ouyang, "A review of electric motor and control technology for rim-driven thruster," *Transactions of China Electrotechnical Society*, Vol. 37, No. 12, 2949–2960, 2022.
2. Yan, X., X. Liang, W. Ouyang, Z. Liu, B. Liu, and J. Lan, "A review of progress and applications of ship shaft-less rim-driven thrusters," *Ocean Engineering*, Vol. 144, 142–156, 2017.
3. Shen, Y., P. Hu, and S. Jin, "Design of novel shaftless pump-jet propulsor for multipurpose long-range and high-speed autonomous underwater vehicle," *IEEE Transactions on Magnetics*, Vol. 52, No. 7, 1–4, 2016.
4. Richardson, K. M., C. Pollock, and J. O. Flower, "Design of a switched reluctance sector motor for an integrated motor/propeller unit," *International Conference on Electrical Machines & Drives*, 271–275, Durham, UK, 1995.
5. Hassannia, A. and A. Darabi, "Design and performance analysis of superconducting rim-driven synchronous motors for marine propulsion," *IEEE Transactions on Applied Superconductivity*, Vol. 24, No. 1, 40–46, 2016.
6. Hang, J., W. Sun, Q. Hu, X. Ren, and S. Ding, "Integration of interturn fault diagnosis and fault-tolerant control for PMSM drive system," *IEEE Transactions on Transportation Electrification*, Vol. 8, No. 2, 2825–2835, 2022.
7. Ma, R., J. Zhu, Q. Lin, and Y. Zhang, "Influence of winding distribution on fault tolerant performance in a fault-tolerant permanent magnet rim driven motor," *IEEE Access*, Vol. 7, 183236–183244, 2019.
8. Qiao, T., J. Zhu, and X. Wang, "Design and optimization of a flux-modulated fault-tolerant permanent magnet rim-driven machine with combined stator to improve torque density," *IEEE Transactions on Energy Conversion*, Vol. 38, No. 1, 75–88, 2023.
9. Teymoori, V., M. Kamper, R.-J. Wang, and R. Kennel, "Sensorless control of dual three-phase permanent magnet synchronous machines — A review," *Energies*, Vol. 16, No. 3, 1326, 2023.
10. Wang, G., M. Valla, and J. Solsona, "Position sensorless permanent magnet synchronous machine drives — A review," *IEEE Transactions on Industrial Electronics*, Vol. 67, No. 7, 5830–5842, 2020.

11. Tir, Z., T. Orlowska-Kowalska, H. Ahmed, and A. Houari, "Adaptive high gain observer based MRAS for sensorless induction motor drives," *IEEE Transactions on Industrial Electronics*, Vol. 71, No. 1, 271–281, 2024.
12. Benevieri, A., A. Formentini, M. Marchesoni, M. Passalacqua, and L. Vaccaro, "Sensorless control with switching frequency square wave voltage injection for SPMSM with low rotor magnetic anisotropy," *IEEE Transactions on Power Electronics*, Vol. 38, No. 8, 10060–10072, 2023.
13. Wen, D., W. Wang, and Y. Zhang, "Sensorless control of permanent magnet synchronous motor in full speed range," *Chinese Journal of Electrical Engineering*, Vol. 8, No. 2, 97–107, 2022.
14. Ye, S. and X. Yao, "An enhanced SMO-based permanent-magnet synchronous machine sensorless drive scheme with current measurement error compensation," *IEEE Journal of Emerging and Selected Topics in Power Electronics*, Vol. 9, No. 4, 4407–4419, 2021.
15. Shuang, B. and Z.-Q. Zhu, "Simultaneous sensorless rotor position and torque estimation for IPMSM at standstill and low speed based on high-frequency square wave voltage injection," *IEEE Transactions on Industrial Electronics*, Vol. 69, No. 9, 8791–8802, 2022.
16. Pacha, M. and S. Zossak, "Improved simple I-F open-loop start-up of PMSM drives without speed or position sensor," *2019 IEEE 10th International Symposium on Sensorless Control for Electrical Drives (SLED)*, 1–6, 2019.
17. Zhang, G., G. Wang, and D. Xu, "Saliency-based position sensorless control methods for PMSM drives — A review," *Chinese Journal of Electrical Engineering*, Vol. 3, No. 2, 14–23, 2017.
18. Sun, J. J., Q. Zhu, Y. Zhou, and J. Zhao, "Open-circuit fault diagnosis of voltage source inverters for PMSM drive system using sine-wave injection method," *2021 33rd Chinese Control and Decision Conference (CCDC)*, 4598–4603, 2021.
19. Liu, J., Y. Zhang, H. Yang, and W. Shen, "Position sensorless control of PMSM drives based on HF sinusoidal pulsating voltage injection," *2020 IEEE Energy Conversion Congress and Exposition (ECCE)*, 3849–3853, 2020.
20. Lu, Q., Y. Wang, L. Mo, and T. Zhang, "Pulsating high frequency voltage injection strategy for sensorless permanent magnet synchronous motor drives," *IEEE Transactions on Applied Superconductivity*, Vol. 31, No. 8, 1–4, 2021.
21. Geng, Q., Z. Li, M. Zhang, Z. Zhou, H. Wang, and T. Shi, "Sensorless control method for dual permanent magnet synchronous motors driven by five-leg voltage source inverter," *IEEE Journal of Emerging and Selected Topics in Power Electronics*, Vol. 10, No. 1, 260–272, 2022.
22. Rahman, A. A., A. Galassini, M. Degano, et al., "Open and short circuit post-fault control strategies for multi-three-phase interior permanent magnet machines," *IEEE Transactions on Energy Conversion*, Vol. 37, No. 1, 163–174, 2022.
23. Gu, L., Q. Chen, W. Zhao, G. Liu, and Y. Xia, "Inter-phase short-circuit fault-tolerant control for five-phase permanent magnet fault-tolerant motors," *Transactions of China Electrotechnical Society*, Vol. 37, No. 8, 1972–1981, 2022.
24. Zhu, J., H. Bai, X. Wang, and X. Li, "Current vector control strategy in a dual-winding fault-tolerant permanent magnet motor drive," *IEEE Transactions on Energy Conversion*, Vol. 33, No. 4, 2191–2199, 2018.